

Even-odd parity effects in Majorana junctions

Alex Zazunov¹, Pasquale Sodano^{2,3} and Reinhold Egger¹

¹ Institut für Theoretische Physik, Heinrich-Heine-Universität, D-40225 Düsseldorf, Germany

² International Institute of Physics, Universidade Federal do Rio Grande do Norte, 59012-970 Natal, Brazil

³ INFN, Sezione di Perugia, Via A. Pascoli, I-06123 Perugia, Italy

E-mail: egger@thphy.uni-duesseldorf.de

Abstract. We study a general Majorana junction, where N helical nanowires are connected to a common s -wave superconductor proximity-inducing Majorana bound states in the wires. The normal part of each wire ($j = 1, \dots, N$) acts as connected lead, where electrons can tunnel into the respective Majorana state $\gamma_{A,j}$. The Majorana states at the other end, $\gamma_{B,j}$, are coupled to each other by an arbitrary tunnel matrix. We examine the conditions for even-odd parity effects in the tunnel conductance for various junction topologies.

Submitted to: *New J. Phys.*

1. Introduction

Since their discovery a few years ago, many fascinating phenomena have been uncovered in topological insulators [1] and topological superconductors [2]. A particularly simple yet nontrivial example is given by the Majorana fermion bound states that must be present near the ends of one-dimensional (1D) topological superconductor wires; for reviews, see Refs. [3, 4, 5]. Since Majorana fermions exhibit non-Abelian statistics, they are under consideration as platforms for topological quantum information processing. An experimental realization in terms of few-channel InSb or InAs nanowires was recently proposed [6, 7], where the conspiracy of pronounced spin-orbit coupling, strong Zeeman magnetic field, and proximity-induced pairing correlations inherited from an s -wave superconducting substrate, will induce the Majorana end states.

Electron tunneling from a normal metal into such a 1D topological superconductor is predicted to show a zero-bias anomaly conductance peak due to resonant Andreev reflection [8, 9, 10, 11, 12, 13, 14, 15, 16]. In essence, the Majorana state delocalizes into the normal metal and forms a resonance pinned to the Fermi energy. This mechanism establishes a perfect Andreev reflection channel, with conductance peak value $G = 2e^2/h$ at temperature $T = 0$. Resonant Andreev reflection is in fact the most important coupling mechanism in such a metal-Majorana contact as long as the proximity-induced

gap exceeds the thermal energy, $k_B T$, and the applied bias voltage scale, eV . All other local perturbations at the contact, e.g., quasi-particle tunneling or potential scattering, were shown to be irrelevant compared to tunneling via the resonant Majorana state [17]. Experimental reports of conductance peaks with such properties in InAs or InSb nanowires (with proximity-induced pairing, strong spin-orbit coupling and appropriate Zeeman fields) have indeed appeared recently [18, 19, 20, 21], possibly providing first experimental signatures for Majoranas. Other Majorana platforms have also been discussed in the literature; for reviews, see Refs. [3, 4, 5].

In order to usefully employ the nonlocal information stored in these Majorana states, one needs to have junctions where at least three Majoranas are coupled [22, 23]. We note in passing that regular 2D Majorana networks, e.g., with many superconducting grains connected by nanowires, can realize exotic spin models such as Kitaev’s toric code [24, 25]. In Majorana junctions, the coupling between Majoranas can either be due to direct tunnel matrix elements, which requires that nanowires are in close proximity to each other, or mediated through the capacitive Coulomb charging energy [26, 27, 28, 29, 30, 31, 32, 33, 34, 35]. In this paper, we study the Majorana junction shown schematically in Fig. 1, where N helical nanowires — where in the simplest case, right-movers have (say) spin up and left-movers spin down [1] — meet on a superconducting electrode. Assuming that the superconductor is grounded, the coupling between Majorana states is modelled phenomenologically by tunnel matrix elements. Note that electron-electron interactions in the normal wire parts may also imply helical Luttinger liquid behavior [1]. Such effects can be included along the lines of Refs. [17, 35], but here we focus on the simplest noninteracting case.

The setup in Fig. 1 provokes the question whether one can observe even-odd parity effects in the tunneling conductance. For tunneling into a chain of Majorana states [12, 36], there indeed is a *strong parity effect*: The $T = 0$ conductance exhibits the unitary zero-bias peak value $G_1(0) = 2e^2/h$ for tunneling into a chain with odd number n of coupled Majoranas, while $G_1(0) = 0$ for even n . Moreover, $n - 1$ zeros and n peaks are present in the bias-dependent $T = 0$ tunneling conductance $G_1(V)$ [12]. The strong parity effect is explained by noting that n coupled Majoranas, for even n , correspond to $n/2$ finite-energy fermion states. The absence of a zero-energy state then implies a quenching of resonant Andreev reflection, and hence $G_1(0) = 0$. For odd n , however, one zero-energy Majorana state remains and allows for perfect Andreev reflection with $G_1(0) = 2e^2/h$. For suitable choices of the tunnel couplings in Eq. (2) below, we will recover these results for the chain topology in Sec. 3.1. At the same time, we will extend them by considering other topologies of the Majorana junction, see Secs. 3.2 and 4. This allows us to study even-odd parity effects in a systematic manner within the general setup of Fig. 1.

The structure of the remainder of this paper is as follows. In Sec. 2, we describe the low-energy model of our Majorana junction and give the formally exact solution for the steady-state currents flowing through the nanowires. This solution is elaborated for the “chain” and “loop” topologies of the junction in Sec. 3, based on analytical results

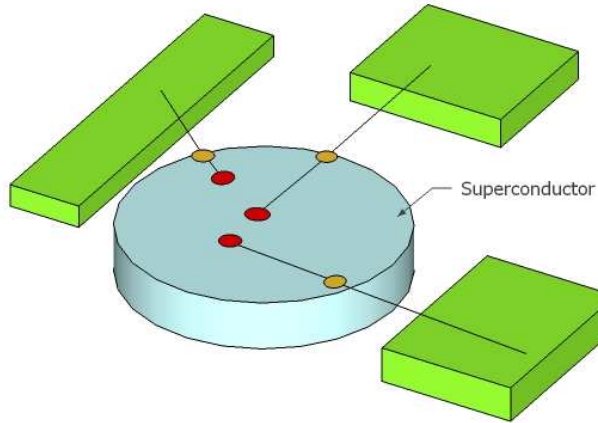


Figure 1. Schematic Majorana junction of N helical nanowires (black lines) connected to a superconducting electrode (blue) and N metal electrodes (green); here $N = 3$. The Majorana states $\gamma_{A,j}$ and $\gamma_{B,j}$ are indicated by yellow and red dots, respectively. Tunneling between different $\gamma_{B,j}$ is encoded in the antisymmetric matrix $\hat{\Omega}$, while t_j refers to the coupling between $\gamma_{A,j}$ and $\gamma_{B,j}$. Tunneling from the j th lead to $\gamma_{A,j}$ is governed by the hybridization $\Gamma_j \propto \lambda_j^2$.

for $N = 2$ and $N = 3$, combined with numerics for arbitrary N . In Sec. 4, we show that analytical progress is possible for additional junction topologies, where N can be arbitrary but $\Gamma_j = \Gamma$ and $t_j = t$. In particular, we address the possibility of parity effects in the tunneling conductance for the “ladder”, “tree,” and “isotropic” junction topologies. Finally, we offer a general interpretation of our results in Sec. 5. Some details have been delegated to the Appendix.

2. Multi-terminal Majorana Junction

2.1. Model

We consider a junction of N helical nanowires ($j = 1, \dots, N$) assembled on top of a conventional s -wave superconducting electrode, see Fig. 1 for a schematic illustration of this multi-terminal Majorana junction. We assume that the superconductor is grounded, and hence charging effects are irrelevant. By virtue of the proximity effect, each nanowire segment located on top of the superconductor turns into a 1D topological superconductor [4]. The bulk-boundary correspondence then implies that there must be a single unpaired Majorana fermion, $\gamma_{B,j}$, at the end of the superconducting wire, plus another one, $\gamma_{A,j}$,

at the interface to the normal part of the wire. The latter part also acts as connected lead and allows to probe electron transport through the multi-terminal Majorana junction in Fig. 1. The Majoranas correspond to self-conjugate operators, $\gamma_{\alpha,j}^\dagger = \gamma_{\alpha,j}$ (with $\alpha = A, B$), subject to the anticommutation relations

$$\{\gamma_{\alpha,j}, \gamma_{\alpha',j'}\} = \delta_{\alpha\alpha'} \delta_{jj'}. \quad (1)$$

It is convenient to combine them to N -component objects, $\gamma_\alpha = (\gamma_{\alpha,1}, \dots, \gamma_{\alpha,N})^T$. Similarly, the conventional lead fermion operators are contained in $c = (c_1, \dots, c_N)^T$, with $c_j = \sum_k c_{jk}$, where c_{jk} annihilates a lead fermion of momentum k in the j th lead. For simplicity, we assume identical dispersion relation ξ_k for all leads, and denote their respective chemical potentials as μ_j (with $\mu_S = 0$ for the superconductor).

Throughout this paper, we focus on the most interesting case where the proximity-induced pairing gap exceeds both the thermal energy, $k_B T$, and the applied bias energies, such that quasi-particle excitations above the gap are negligible. Retaining only the Majoranas as relevant fermionic degrees of freedom for the junction in Fig. 1, the Hamiltonian reads

$$H = H_l + \frac{i}{2} \gamma_B \hat{\Omega} \gamma_B + i \gamma_A \hat{t} \gamma_B + (c^\dagger - c) \hat{\lambda} \gamma_A, \quad (2)$$

where $H_l = \sum_{j=1}^N \sum_k \xi_k c_{jk}^\dagger c_{jk}$ describes the leads. The ‘‘hat’’ notation in Eq. (2) refers to an $N \times N$ matrix structure in wire-number (j) space. Without loss of generality, the antisymmetric matrix $\hat{\Omega}$, containing the couplings between different $\gamma_{B,j}$, is chosen real-valued. The same holds true for the tunnel couplings t_j , connecting $\gamma_{A,j}$ and $\gamma_{B,j}$ in the j th wire, and for λ_j , connecting $\gamma_{A,j}$ to the lead fermion c_j ; we use $\hat{t} = \text{diag}(t_1, \dots, t_N)$ and $\hat{\lambda} = (\lambda_1, \dots, \lambda_N)$. Within the standard wide-band approximation for the leads [37], the λ_j only appear through the hybridization scales $\Gamma_j = 2\pi\nu_0\lambda_j^2$, where $\hat{\Gamma} = (\Gamma_1, \dots, \Gamma_N)$ and $\nu_0 = \sum_k \delta(\xi_k)$ is the constant lead density of states. By putting some of the couplings $\{\Gamma_j, t_j, \Omega_{j<j'}\}$ to zero, Eq. (2) serves as a general model for $M \leq N$ normal-metal terminals connected through a junction of $n \leq 2N$ coupled Majorana fermions. The aim of this paper is to quantitatively understand the tunneling current into such a multi-terminal Majorana junction.

2.2. Conductance

The stationary current flowing in the j th nanowire towards the junction, I_j , follows from the relation [12, 30]

$$I_j = \frac{e\Gamma_j}{h} \int d\epsilon F(\epsilon - \mu_j) \text{Im} \mathcal{G}_{A_j, A_j}^r(\epsilon), \quad (3)$$

where we have Fermi distributions in the leads, $F(\epsilon) = \tanh(\epsilon/2k_B T)$, and $\mathcal{G}_{\alpha_j, \alpha'_j}^r(\epsilon)$ is the energy representation of the retarded Majorana Green’s function. The main quantity of interest in experiments is the corresponding differential conductance $G_j = e\partial I_j / \partial \mu_j$, which yields from Eq. (3) the $T = 0$ result

$$G_j = \frac{2e^2}{h} \Gamma_j [-\text{Im} \mathcal{G}_{A_j, A_j}^r(\mu_j)]. \quad (4)$$

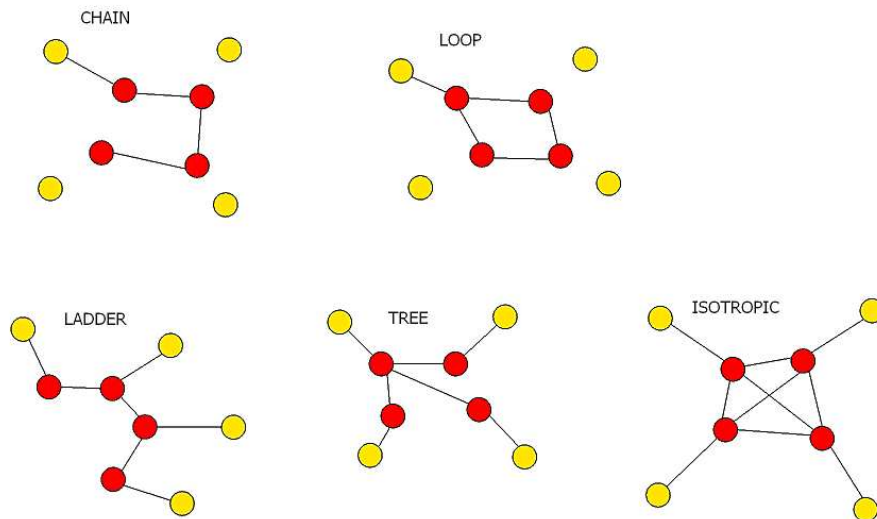


Figure 2. Different topologies of a Majorana junction, shown here for $N = 4$. Yellow (red) dots refer to $\gamma_{A,j}$ ($\gamma_{B,j}$) Majorana states, with the respective top left state for $j = 1$. A line connecting two dots indicates that the respective coupling t_j or $\Omega_{j,k}$ is finite.

Since we have a noninteracting Hamiltonian in Eq. (2), the Dyson equation for \mathcal{G}^r can be solved exactly. As sketched in the Appendix, the $2N \times 2N$ matrix for \mathcal{G}^r thereby takes the form (the 2×2 block structure refers to $\alpha = A, B$ space)

$$\mathcal{G}^r(\epsilon) = \begin{pmatrix} \epsilon \hat{1} + i\hat{\Gamma} & -i\hat{t} \\ i\hat{t} & \epsilon \hat{1} - i\hat{\Omega} \end{pmatrix}^{-1}, \quad (5)$$

where $\hat{1}$ is the $N \times N$ unit matrix in wire-number space. The matrix element $\mathcal{G}_{A_j, A_j}^r(\epsilon)$ obtained from Eq. (5) then determines the current I_j and hence the conductance G_j .

Current conservation, $\sum_{j=1}^N I_j = 0$, is *not* imposed here due to the presence of a grounded superconductor [8]. Since the retarded Green's function in Eq. (5) does not depend on the chemical potentials, the current I_j , and hence also the conductance G_j , depends on the respective chemical potential μ_j only, but not on the $\mu_{k \neq j}$. All “nonlocal” conductances, $e\partial I_j / \partial \mu_{k \neq j}$, therefore vanish identically regardless of the values of the tunnel couplings, as long as the validity requirements for Eq. (2) are met. The resulting decoupling of different terminals is a characteristic feature of noninteracting Majorana networks and can be traced back to the assumption of a *grounded* superconductor. For a “floating” (not grounded) mesoscopic superconductor, where current must be conserved and Coulomb charging effects may become important, nonlocal conductances are typically finite.

From now on, without loss of generality, we consider only the tunneling conductance $G_1(V) = dI_1(V)/dV$ for nanowire $j = 1$, with $eV \equiv \mu_1$ and in the most interesting $T = 0$

limit, see Eq. (4). It is worth stressing that while G_1 is independent of the chemical potentials $\mu_{j>1}$, it still does depend on all hybridization parameters Γ_j . Although $G_1(V)$ can always be expressed in terms of the retarded Green's function (5), explicit results for arbitrary parameters are generally lengthy and not illuminating. We here instead aim at analytical results by examining several limiting cases for the specific junction topologies drawn in Fig. 2. In Sec. 3, we consider $N = 2$ nanowires with arbitrary coupling matrix elements, where a compact expression for $G_1(V)$ allows us to study tunneling into a “chain” of Majoranas. The case of $N = 3$ wires is also addressed, where we obtain insights for the “loop” geometry in Fig. 2. We then analyze the linear conductance $G_1(0)$ for loop configurations with arbitrary $N > 2$ Majorana states in the loop and study the parity effect for such a junction topology. In Sec. 4, we discuss the remaining three topologies shown in Fig. 2, where we assume $\Gamma_j = \Gamma$ and $t_j = t$ in order to simplify the analysis. In addition, all non-zero matrix entries in $\hat{\Omega}$ are assumed equal, i.e., $\Omega_{j<k}$ is either some finite constant (Ω) or zero. Under these conditions, we show that analytical results for $G_1(V)$ with arbitrary N can be derived, which allows us to systematically study even-odd parity effects in Majorana junctions. Before moving on, however, we first discuss a useful reformulation of Eq. (5).

2.3. Retarded Green's function

To achieve analytical progress for arbitrary N , at least for some special parameter choices in Eq. (2), it is convenient to write the relevant matrix element, $\mathcal{G}_{A1,A1}^r(\epsilon)$, of the retarded Green's function in an alternative form avoiding direct matrix inversion. We first single out the effects of the inter-wire couplings $\hat{\Omega}$ by writing a Dyson equation for \mathcal{G}^r ,

$$\mathcal{G}^r = \mathcal{G}_0^r + \mathcal{G}_0^r \begin{pmatrix} 0 & 0 \\ 0 & i\hat{\Omega} \end{pmatrix} \mathcal{G}^r, \quad (6)$$

where the “unperturbed” ($\hat{\Omega} = 0$) retarded Green's function \mathcal{G}_0^r is diagonal in wire-number space. In fact, we can read off its matrix elements from Eq. (5),

$$[\mathcal{G}_0^r(\epsilon)]_{\alpha j, \alpha' j'} = \frac{\delta_{jj'}}{\epsilon^2 - t_j^2 + i\epsilon\Gamma_j} \begin{pmatrix} \epsilon & it_j \\ -it_j & \epsilon + i\Gamma_j \end{pmatrix}_{\alpha, \alpha'}. \quad (7)$$

Now we introduce the auxiliary quantities

$$X_j(\epsilon) \equiv \frac{\mathcal{G}_{Bj,A1}^r(\epsilon)}{[\mathcal{G}_0^r]_{B1,A1}(\epsilon)}, \quad (8)$$

which encode the off-diagonal matrix elements of the retarded Green's function and fulfill the relation

$$X_j - i \frac{\epsilon + i\Gamma_j}{\epsilon^2 - t_j^2 + i\epsilon\Gamma_j} \sum_{k=1}^N \Omega_{jk} X_k = \delta_{j,1}. \quad (9)$$

Equation (9) follows by taking the $(Bj, A1)$ matrix element of Eq. (6), and is widely used below to determine the X_j . Note that for the tunneling conductance (4) we need $\mathcal{G}_{A1,A1}^r(\epsilon)$. Taking the $(A1, A1)$ matrix element of Eq. (6) yields after some algebra

$$\mathcal{G}_{A1,A1}^r(\epsilon) = \frac{1}{\epsilon + i\Gamma_1} \left(1 + \frac{t_1^2 X_1(\epsilon)}{\epsilon^2 - t_1^2 + i\epsilon\Gamma_1} \right). \quad (10)$$

Equation (10) can be further simplified for $\epsilon = eV \rightarrow 0$, where the *linear conductance* is

$$G_1(0) = \frac{2e^2}{h} (1 - X_1). \quad (11)$$

The real-valued $X_1 = X_1(\epsilon = 0)$ follows from solving Eq. (9).

3. Chain and loop junctions

3.1. Conductance for chain topology

Let us start with the case of $N = 2$ nanowires, where $\hat{\Omega}$ is fully determined by just one parameter, $\Omega_{12} = \Omega$. Equation (5) then yields the Green's function matrix element determining the tunneling conductance,

$$\mathcal{G}_{A1,A1}^r(\epsilon) = \frac{\epsilon t_2^2 + (\Omega^2 - \epsilon^2)(\epsilon + i\Gamma_2)}{\Omega^2(\epsilon + i\Gamma_1)(\epsilon + i\Gamma_2) - (\epsilon^2 - t_1^2 + i\epsilon\Gamma_1)(\epsilon^2 - t_2^2 + i\epsilon\Gamma_2)}. \quad (12)$$

Several remarks about this result are in order. (i) For $t_1 = 0$, Eq. (12) reduces to $\mathcal{G}_{A1,A1}^r = 1/(\epsilon + i\Gamma_1)$, which leads to the well-known resonant Andreev reflection peak for tunneling into a single decoupled Majorana fermion (γ_{A1}) [8, 11],

$$G_1(V) = \frac{2e^2}{h} \frac{\Gamma_1^2}{\Gamma_1^2 + (eV)^2}. \quad (13)$$

Note that the parameters t_2 and Γ_2 do not affect this result at all. (ii) Without coupling between the wires, $\Omega = 0$, but with $t_1 \neq 0$, the Majorana $\gamma_{B,1}$ is also involved and the resonance (13) will split into two symmetric finite-voltage peaks separated by a perfect dip at zero bias [8, 11]. Indeed, now Eq. (12) yields

$$G_1(V) = \frac{2e^2}{h} \frac{(eV\Gamma_1)^2}{(eV\Gamma_1)^2 + [(eV)^2 - t_1^2]^2}, \quad (14)$$

such that the linear ($V \rightarrow 0$) conductance vanishes but two perfect ($G_1 = 2e^2/h$) peaks are present for $eV = \pm t_1$. This reflects the parity effect in a chain of n coupled Majoranas, where $G_1(V)$ has $n - 1$ zeroes and n unitary peaks [12], in accordance with Eq. (14) for $n = 2$. (iii) Putting $t_2 = 0$ in Eq. (12), we effectively recover tunneling into the $n = 3$ Majorana chain composed by $\gamma_{A1} - \gamma_{B1} - \gamma_{B2}$,

$$G_1(V) = \frac{2e^2}{h} \frac{\Gamma_1^2[\Omega^2 - (eV)^2]^2}{(eV)^2[\Omega^2 + t_1^2 - (eV)^2]^2 + \Gamma_1^2[\Omega^2 - (eV)^2]^2}, \quad (15)$$

which exhibits three unitary conductance peaks, at $V = 0$ and $eV = \pm\sqrt{\Omega^2 + t_1^2}$, and two zeroes, $eV = \pm\Omega$, as expected under the parity effect. (iv) Finally, the $n = 4$

Majorana chain is realized for $\Gamma_2 = 0$ in Eq. (12). For simplicity, we put $t_1 = t_2 = t$ and obtain

$$G_1 = \frac{2e^2}{h} \frac{(eV\Gamma_1)^2[\Omega^2 + t^2 - (eV)^2]^2}{[(eV)^2\Omega^2 - ((eV)^2 - t^2)^2] + (eV\Gamma_1)^2[\Omega + t^2 - (eV)^2]^2}. \quad (16)$$

Clearly, we have three zeroes, $V = 0$ and $eV = \pm\sqrt{\Omega^2 + t^2}$, and four unitary conductance peaks, $eV = \pm\frac{\Omega}{2} \pm \sqrt{\Omega^2/4 + t^2}$ with independent \pm signs. When also $\Gamma_2 \neq 0$, the parity effect is not ideal anymore, i.e. peak conductances are smaller than $2e^2/h$, but it remains observable.

The above Majorana chain configuration can be generalized to setups with $N > 2$ and $n \leq N + 1$ Majorana states, see Fig. 2. Let us focus on computing the linear conductance $G_1(0)$ for $n = N + 1$. To that end, we put $t_{j>1} = 0$ and keep as non-zero entries in $\hat{\Omega}$ only the nearest-neighbor couplings $\Omega_{j,j+1}$ with $j = 1, \dots, N - 1$. In the limit $\epsilon \rightarrow 0$, the Dyson equation (9) yields

$$X_1 - \frac{\Gamma_1\Omega_{12}}{t_1^2} X_2 = 1, \quad \Omega_{j,j+1}X_{j+1} + \Omega_{j,j-1}X_{j-1} = 0 \quad (17)$$

for $j = 2, \dots, N$. The boundary condition $X_{N+1} = 0$ leads to $X_{j \text{ odd}} = 0$ ($X_{j \text{ even}} = 0$) for even (odd) N , and hence $X_1 = \delta_{N,\text{odd}}$. The conductance (11) for tunneling into this chain of $n = N + 1$ Majoranas is

$$G_1(0) = \frac{2e^2}{h} \delta_{n,\text{odd}}, \quad (18)$$

and exhibits a strong parity effect. Moreover, we have numerically confirmed the strong parity effect in such a junction by computing the differential conductance. In full agreement with Ref. [12], we found that $G_1(V)$ exhibits n unitary-limit ($2e^2/h$) peaks as a function of bias V .

3.2. Conductance for loop topology

The algebra needed to obtain $G_1(V)$ from Eq. (5) for $N > 2$ Majorana wires becomes much more involved. For $N = 3$, the linear conductance can still be given in compact form for arbitrary parameters. We find:

$$G_1(0) = \frac{2e^2}{h} \frac{\Gamma_1\xi}{\Gamma_1\xi + t_1^2(t_2^2t_3^2 + \Gamma_2\Gamma_3\Omega_{23}^2)}, \quad \xi = \Omega_{12}^2\Gamma_2t_3^2 + \Omega_{13}^2\Gamma_3t_2^2. \quad (19)$$

For $t_1 \neq 0$, the unitary limit ($G_1 = 2e^2/h$) is reached when either $t_2 = \Gamma_3\Omega_{23} = 0$ or $t_3 = \Gamma_2\Omega_{23} = 0$, while at the same time $\xi \neq 0$. Note that $G_1(0) = 0$ when $t_2 = t_3 = 0$. The junction then consists of γ_{A1} coupled to a closed ‘‘loop’’ consisting of the three B Majoranas. This is the simplest example for the ‘‘loop’’ topology shown in Fig. 2.

The linear conductance $G_1(0)$ for loop junction configurations with arbitrary $N > 2$ and non-vanishing $\Omega_{j,j+1}$ can readily be analyzed using the Dyson equation (9). As before, see Sec. 3.1, assuming $t_j = t_1\delta_{j,1}$ and taking the limit $\epsilon \rightarrow 0$ in Eq. (9), we obtain

$$X_1 - \frac{\Gamma_1}{t_1^2} (\Omega_{12}X_2 + \Omega_{1N}X_N) = 1, \quad \Omega_{j,j+1}X_{j+1} + \Omega_{j,j-1}X_{j-1} = 0 \quad (20)$$

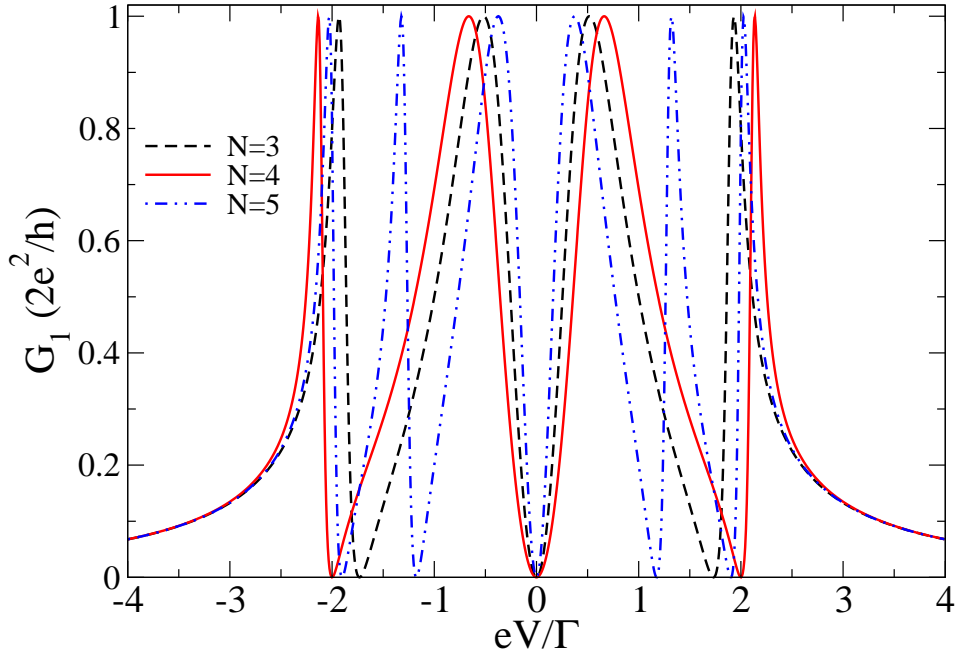


Figure 3. Tunneling conductance $G_1(V)$ vs. eV/Γ (with $\Gamma = \Gamma_1$) for a Majorana junction in the homogeneous “loop” configuration ($\Omega_{j,j+1} = \Omega$), shown for several N with $t_1/\Gamma = \Omega/\Gamma = 1$.

for $j = 2, \dots, N$, with periodic boundary conditions, $X_{N+1} = X_1$. For odd N , one can verify that Eq. (20) has always, i.e., for arbitrary $\Omega_{j,j+1}$, the solution $X_1 = 1$. Indeed, for $X_1 = 1$, the two sequences X_j odd/even, both obeying

$$X_j = \frac{\Omega_{j-2,j-1}}{\Omega_{j-1,j}} X_{j-2} \quad (21)$$

with $j \neq 1 \pmod{N}$, are uniquely determined by virtue of the matching relation $\Omega_{12}X_2 + \Omega_{1N}X_N = 0$. As a result, the linear conductance (11) always vanishes for odd N . For even N , a general solution to Eq. (20) is given by

$$\begin{aligned} X_{j \text{ odd}} &= 0, \\ X_{j \text{ even}} &= \frac{\Omega_{j-2,j-1}}{\Omega_{j-1,j}} X_{j-2}, \\ \Omega_{12}X_2 + \Omega_{1N}X_N &= -t_1^2/\Gamma_1, \end{aligned} \quad (22)$$

implying that the linear conductance (11) reaches the unitary-limit value $2e^2/h$. This suggests that like for a Majorana chain, the strong parity effect described by Eq. (18) with $n = N + 1$ is also present for the loop topology. Thus, by changing the number of tunnel coupled nanowires N in the loop configuration, one may switch the conductance $G_1(0)$ on and off, depending on the parity of N . This parity-based switching mechanism for the tunneling conductance stems from the non-local nature of electron transport in Majorana junctions, and offers a way to “engineer” such parity effects.

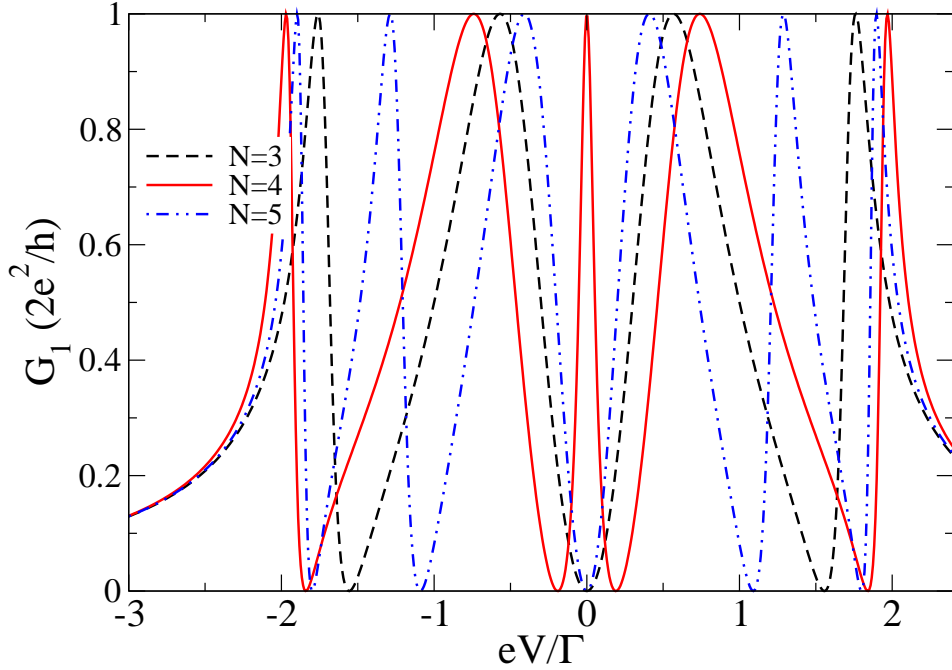


Figure 4. Same as in Fig. 3 but for generic inhomogeneous “loop” configuration, where only $\Omega_{1,2} = 0.65\Gamma_1$ has been changed; all other $\Omega_{i,i+1} = \Gamma_1$ as in Fig. 3.

However, the solution (22) fails when N is even and the parameters $\Omega_{j,j+1}$ satisfy the incompatibility condition

$$\Omega_{12} + \Omega_{1N} \prod_{k=1}^{N/2-1} \frac{\Omega_{2k,2k+1}}{\Omega_{2k+1,2k+2}} = 0. \quad (23)$$

In particular, for a homogeneous loop configuration with identical couplings [$\Omega_{j,j+1} = \Omega$ for all j], Eq. (23) is satisfied. We then have the trivial solution $X_j = 1$ for all j , regardless of the parity of $N > 2$. Consequently, $G_1(0) = 0$ for arbitrary (odd or even) number of Majoranas in such a loop. This can be understood as a result of the destructive interference – with complete cancellation of clockwise and anti-clockwise contributions to $G_1(0)$ – in a homogeneous Majorana loop (closed chain).

Remarkably, for even N and arbitrary Majorana loops, this interference therefore results in either a maximal ($G_1 = 2e^2/h$) or a completely blocked ($G_1 = 0$) zero-bias conductance, depending on the incompatibility condition in Eq. (23). Fig. 3 shows the differential conductance $G_1(V)$ for several N in the homogeneous loop configuration. Numerically, we find that the number P of finite-bias peaks in $G_1(V)$ for this configuration is given by

$$P = \begin{cases} N + 1, & N \text{ odd,} \\ 2(1 + [N/4]), & N \text{ even,} \end{cases} \quad (24)$$

with $[x]$ denoting the integer part of x . Due to the lack of an unambiguous correspondence between P and N , a parity effect is difficult to detect in the homogeneous loop.

Let us stress again that in the loop configuration, $G_1(V)$ exhibits the strong parity effect, with $N + 1$ unitary-limit ($2e^2/h$) peaks as in the chain configuration, for generic (inhomogeneous) parameters. This is illustrated in Fig. 4 for a particular choice of the $\Omega_{i,i+1}$ couplings.

4. Junction topologies and parity effects

In this section, we address the three remaining junction topologies in Fig. 2 for arbitrary N . The tunneling conductance is obtained for a parameter set with equal hybridizations, $\Gamma_j = \Gamma$, and intra-wire couplings, $t_j = t$. The matrix elements $\Omega_{j<k}$ are either zero or equal to a single constant (Ω), depending on the junction type.

4.1. Ladder configuration

For the “ladder” shown in Fig. 2, the only non-zero $\Omega_{j<k}$ entries are nearest-neighbor bonds, $\Omega_{j,j+1} = \Omega$ for $j = 1, \dots, N$ (“closed ladder”) or $j = 1, \dots, N - 1$ (“open ladder”). The example shown in Fig. 2 refers to an open ladder for $N = 4$. For both ladder configurations, Eq. (9) for $X_j(\epsilon)$ takes the form

$$X_j - A(X_{j+1} - X_{j-1}) = \delta_{j,1}, \quad A(\epsilon) = \frac{i\Omega(\epsilon + i\Gamma)}{\epsilon^2 - t^2 + i\epsilon\Gamma}, \quad (25)$$

supplemented by the boundary conditions $X_0 = X_{N+1} = 0$ ($X_j = X_{j+N}$) for the open (closed) ladder configuration.

Starting with the *open ladder*, the solution of Eq. (25) is

$$X_1(\epsilon) = \frac{\sqrt{1 + 4A^2} F_+^{N+1} + F_-^{N+1}}{2A^2} - \frac{1}{2A^2}, \quad F_{\pm}(\epsilon) = \frac{1 \pm \sqrt{1 + 4A^2}}{2A}. \quad (26)$$

The conductance $G_1(V)$ follows readily from Eqs. (4) and (10). For $N \gg 1$, using $|F_+/F_-| > 1$, we find that X_1 in Eq. (26) becomes N -independent, $X_1 \simeq -F_-/A$. Hence N -dependent parity effects must disappear in this junction type for large N . However, for moderate N , we still observe even-odd parity effects, see Fig. 5. For odd (even) N , $G_1(V)$ exhibits a dip (peak) near zero bias. However, peaks do not reach the unitary limit ($G_1 = 2e^2/h$) and dips are not associated with perfect conductance zeroes anymore. We call this behavior “*weak parity effect*” to contrast it from the ideal “strong parity effect” found for tunneling into a Majorana chain or loop, see Sec. 3. Notice that the even-odd features, clearly visible in the lower inset in Fig. 5 for the linear conductance, gradually disappear as N increases, as expected from the above argument. The upper right inset of Fig. 5 shows that the linear conductance $G_1(0)$ monotonically increases with the effective parameter $A(0) = \Omega\Gamma/t^2$. The tunnel couplings in our model enter $G_1(0)$ in this configuration only through $A(0)$.

For the *closed ladder*, we find a very similar picture. Now the solution to Eq. (25) follows by Fourier expansion,

$$X_1(\epsilon) = \frac{1}{N} \sum_{m=-N}^{N-1} \frac{1}{1 - 2iA(\epsilon) \sin(\pi m/N)}. \quad (27)$$

Eve:

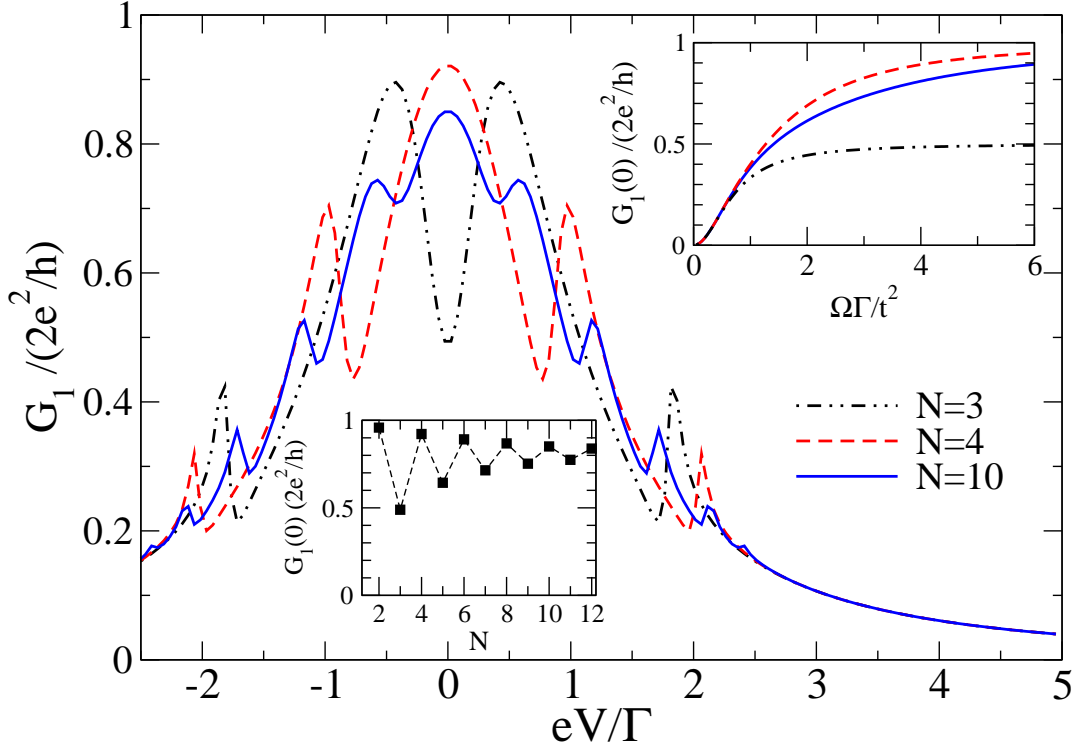


Figure 5. Differential conductance $G_1(V)$ for tunneling into a Majorana junction in the “open ladder” configuration. Main panel: G_1 vs. eV/Γ with $t/\Gamma = 0.5$, $\Omega/\Gamma = 1.2$ and several N . Upper right inset: Linear conductance $G_1(0)$ vs. $\Omega\Gamma/t^2$ for $N = 3, 4$, and 10 . Lower inset: N -dependence of $G_1(0)$ for same parameters.

In the large- N limit, this expression turns into an N -independent integral and parity effects are quenched. Numerical evaluation [based on Eqs. (4), (10) and (27)] shows that the differential conductance $G_1(V)$ has P peaks, where the number P coincides with the one found in the homogeneous loop configuration, see Eq. (24). However, now the peak structure is less pronounced.

To conclude, a Majorana junction with ladder topology, either of closed or open type, is found to exhibit a weak even-odd parity effect that disappears for $N \rightarrow \infty$.

4.2. Tree configuration

Next we study the “tree” topology in Fig. 2, where $\gamma_{B,1}$ is connected to all other $\gamma_{B,j>1}$ through $\Omega_{1,j} = \Omega$, but the remaining $\hat{\Omega}$ -couplings vanish. Now Eq. (9) has the solution

$$X_1(\epsilon) = \left(1 - \frac{(N-1)\Omega^2(\epsilon + i\Gamma)^2}{(\epsilon^2 - t^2 + i\epsilon\Gamma)^2} \right)^{-1}. \quad (28)$$

The linear conductance then follows from Eq. (11),

$$G_1(0) = \frac{2e^2}{h} \left(1 + \frac{t^4}{(N-1)\Omega^2\Gamma^2} \right)^{-1}. \quad (29)$$

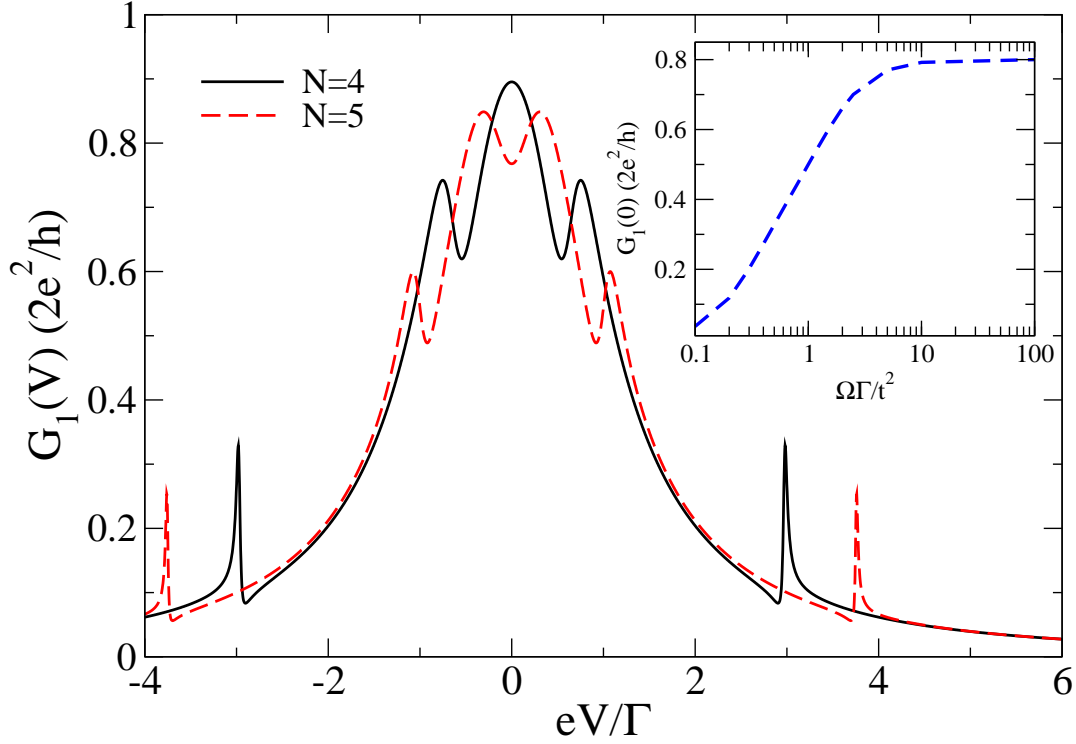


Figure 6. $G_1(V)$ for the “isotropic” case with $N = 4$ and $N = 5$, for $t/\Gamma = 0.5$ and $\Omega/\Gamma = 1.2$. Inset: Linear conductance $G_1(0)$ vs. $A = \Omega\Gamma/t^2$ for $N = 5$.

There is no oscillatory (even-odd) N -dependence, and we find *no parity effect* in the tree configuration. Interestingly, as N increases, $\gamma_{A,1}$ effectively decouples and the unitary single-Majorana limit is approached.

4.3. Isotropic configuration

Finally, consider the isotropic configuration in Fig. 2, where all couplings $\Omega_{j<k} = \Omega$ have the same magnitude. (Note that similar isotropic couplings also arise through the charging interaction [34, 35].) As detailed in the Appendix, for the isotropic Majorana junction with arbitrary N , the tunneling conductance is given by

$$G_1(V) = \frac{2e^2}{h} \text{Im} \left[-\frac{\Gamma}{\epsilon + i\Gamma} \left(1 + \frac{t^2 X_1(\epsilon)}{\epsilon^2 - t^2 + i\epsilon\Gamma} \right) \right]_{\epsilon=eV},$$

$$X_1(\epsilon) = \frac{1}{1 + \left(1 - \frac{1}{\xi_1(\epsilon)} \right) A(\epsilon)}, \quad (30)$$

where $A(\epsilon) = i\Omega(\epsilon + i\Gamma)/(\epsilon^2 - t^2 + i\epsilon\Gamma)$ is as in Eq. (25) for the ladder topology, and

$$\xi_1(\epsilon) = \frac{1}{2} \left[1 + \left(\frac{1 + A(\epsilon)}{1 - A(\epsilon)} \right)^{N-1} \right]. \quad (31)$$

The nonlinear tunneling conductance $G_1(V)$ is shown in Fig. 6. It exhibits a weak parity effect, with a zero-bias peak (dip) in $G_1(V)$ for even (odd) N . In particular, the dip

does not lead to a perfectly vanishing linear conductance.

To study this issue in more detail, note that for $\epsilon = eV = 0$ one has $A = \Omega\Gamma/t^2$ and the linear conductance is given by Eq. (11). For $A \gg N$, Eq. (31) implies $\xi_1 \approx \delta_{N,\text{odd}} + (-1)^{N-1}(N-1)/A$, and hence we get in this limit $X_1 \simeq \delta_{N,\text{odd}}/N$, i.e.,

$$G_1(0) \simeq \frac{2e^2}{h} \left(1 - \frac{\delta_{N,\text{odd}}}{N} \right). \quad (32)$$

The linear conductance thus exhibits a parity effect for $\Omega\Gamma/t^2 \gg 1$. However, this effect disappears for large N . The approach to Eq. (32) with growing A is shown in the inset of Fig. 6 for $N = 5$.

We conclude that the isotropic Majorana junction is characterized by a *weak parity effect* for small-to-intermediate N , quite similar to the ladder configuration in Sec. 4.1.

5. Discussion and conclusions

We now offer an intuitive and general interpretation of our results for the linear tunneling conductance $G_1 = G_1(0)$, where lead $j = 1$ is connected to a set \mathcal{M} of coupled Majorana fermions. Every Majorana fermion in the set \mathcal{M} is linked to other Majoranas in this set through $K = 1, 2, \dots$ “bonds”, where a bond requires that the respective tunnel coupling is finite. In general, the set \mathcal{M} contains not only the $\gamma_{\alpha,j}$ but also additional Majorana fermions $\eta_j \propto c_j - c_j^\dagger$ corresponding to the normal parts (leads). The η_j are coupled only to $\gamma_{A,j}$ by λ_j , see Eq. (2), with $\Gamma_j \propto \lambda_j^2$. We note in passing that within the bosonization approach, the η_j represent Klein factors for each lead [34, 35]. A Majorana mode with $K = 1$ (but not η_1) is called “outer Majorana fermion” and, if present, constitutes a boundary of the set \mathcal{M} . The tunneling conductance G_1 then follows by summing over all propagation amplitudes for paths on \mathcal{M} connecting η_1 and outer Majoranas, where a possible parity effect follows from the following rule: *Trajectories containing an odd (even) number of Majoranas in the set \mathcal{M} yield a finite (zero) contribution to G_1 .* If \mathcal{M} has no boundary (i.e., no outer Majoranas exist), G_1 is determined by the sum over all “loop” trajectories passing through $\gamma_{A,1}$. In particular, “homogeneous loop” trajectories do not contribute to G_1 , see our analysis in Sec. 3.2.

We have verified this rule for the case of $N = 3$ nanowires (for arbitrary parameters) in Sec. 3.1 as well as for all the examples in Sec. 4. For instance, in the “tree” configuration, Eq. (29) shows that $G_1 \neq 0$ for arbitrary N . Since there are $N - 1$ outer Majoranas $\eta_{j>1}$, each connected to η_1 through a chain of four Majoranas, every path connecting η_1 and $\eta_{j>1}$ involves an odd number (five) of Majoranas. (Note that η_1 is not included in the set \mathcal{M} , and hence, in the Majorana number, it should not be counted while the outer Majorana $\eta_{j>1}$ counts.) As a result, a finite conductance G_1 follows from the above rule. As another example, consider the “ladder” configuration with N wires, where we also have $N - 1$ outer Majoranas ($\eta_{j>1}$). Here, paths connecting η_1 and η_m , for even $m = 2, 4, \dots$, lead to an enhancement of G_1 , which can explain the reported peak *vs.* dip structure for even *vs.* odd N .

The present work has shown that rich parity effects are present in junctions of multiple Majorana nanowires. For chain-like arrangements, the $T = 0$ linear tunneling conductance is either zero (for even number of Majoranas) or $2e^2/h$ (for odd number) [12]. Such a strong parity effect does not survive for general junction topologies. For instance, in the “ladder” and “isotropic” topologies, see Fig. 2, one has only a “weak parity effect”, where non-ideal zero-bias dips and peaks can be observed in the tunneling conductance depending on the parity of the Majorana number. However, these effects are less pronounced and disappear with increasing number of Majoranas. In other configurations, e.g., for the “tree” topology, there is no parity effect at all. A particularly noteworthy result concerns the tunneling conductance when $\gamma_{A,1}$ is coupled to a “Majorana loop.” For generic parameters, a strong parity effect is present for such a junction topology, with the even-odd features in the conductance as for a Majorana chain. However, for a homogeneous loop (and in some other special cases), the linear conductance is found to vanish for any number of Majorana fermions in the loop, i.e., no parity effect can be detected.

Finally, let us briefly address the role of finite-temperature effects and of Coulomb interactions. Finite T implies a thermal broadening of all peak or dip features in the differential conductance, plus a reduction of the peaks. Once T reaches the energy scale corresponding to the separation between two adjacent peaks in $G_1(V)$, peaks start to overlap and the parity effects described here will be smeared out. Concerning Coulomb interactions, it has recently been pointed out that charging effects cause interesting Kondo physics in similar Majorana networks [32, 34, 35]. This physics is different from the parity effects studied here, and it would be interesting to study their interplay with Kondo physics for finite charging energy.

Acknowledgments

We acknowledge support by the DFG within the research networks SFB TR 12 and SPP 1666, and by the Ministry of Science, Technology and Innovation of Brazil.

Appendix

Retarded Majorana Green's function

Here we briefly sketch the derivation of Eq. (5), obtained by solving the combined equations of motion for Majoranas and lead fermions,

$$i\partial_t\gamma_{A,j} = it_j\gamma_{B,j} + \lambda_j(c_j - c_j^\dagger), \quad i\partial_t\gamma_{B,j} = -it_j\gamma_{A,j} + i\sum_{j'}\Omega_{jj'}\gamma_{B,j'},$$

$$(i\partial_t - \xi_k)c_{kj} = \lambda_j\gamma_{A,j}.$$

The retarded Green's function is contained in the general Keldysh Green's function

$$\mathcal{G}_{\alpha_j,\alpha'_{j'}}(t,t') = -\frac{i}{\hbar}\langle\mathcal{T}_C\gamma_{\alpha,j}(t)\gamma_{\alpha'_{j'}}(t')\rangle,$$

where \mathcal{T}_C denotes time ordering along the standard Keldysh contour [37]. Exploiting the wide-band approximation for the leads, some algebra yields the Dyson equation for \mathcal{G} from the above equations of motion,

$$\begin{pmatrix} \epsilon\hat{1} - \hat{\Sigma}(\epsilon) & -i\hat{t} \\ i\hat{t} & \epsilon\hat{1} - i\hat{\Omega} \end{pmatrix} \mathcal{G}(\epsilon) = \begin{pmatrix} \hat{1} & 0 \\ 0 & \hat{1} \end{pmatrix}.$$

The 2×2 structure refers to $\alpha = A, B$ space. In addition, every matrix entry still carries the standard 2×2 Keldysh substructure [37], $\mathcal{G} = \begin{pmatrix} \mathcal{G}^r & \mathcal{G}^K \\ 0 & \mathcal{G}^a \end{pmatrix}$, where $\mathcal{G}^a = [\mathcal{G}^r]^\dagger$ and the Keldysh component is \mathcal{G}^K . The Keldysh structure of the self-energy $\hat{\Sigma}(\epsilon) = \text{diag}(\Sigma_1, \dots, \Sigma_N)$ due to the lead fermions is

$$\Sigma_j(\epsilon) = -i\Gamma_j \begin{pmatrix} 1 & F(\epsilon - \mu_j) + F(\epsilon + \mu_j) \\ 0 & -1 \end{pmatrix},$$

where $F(\epsilon) = \tanh(\epsilon/2k_B T)$. Noting that $\hat{\Omega}$ and \hat{t} are diagonal matrices in Keldysh space, it is then straightforward to extract the $2N \times 2N$ matrix for the retarded Green's function \mathcal{G}^r quoted in Eq. (5).

Isotropic junction

Here we show how to derive the quantity $X_1(\epsilon)$ quoted in Eq. (30) for the isotropic topology in Sec. 4.3. First, it is useful to define auxiliary variables $Y_j(\epsilon) = \sum_{k=1}^j X_k(\epsilon)$ for $j = 0, \dots, N$, with $Y_0 \equiv 0$. The Dyson equation for X_j , see Eq. (9), then takes the form

$$(1 + A)Y_j - (1 - A)Y_{j-1} = \delta_{j,1} + AY_N,$$

with $A(\epsilon)$ specified in Eq. (25). For $j = 1$, this reduces to

$$Y_1 = \frac{1 + AY_N}{1 + A},$$

while for $j > 1$, we arrive at a non-homogeneous linear recursion relation for the quantities $\xi_j \equiv Y_j/Y_N$,

$$(1 + A)\xi_j - (1 - A)\xi_{j-1} = A, \quad \xi_N = 1.$$

One can easily verify that this set of equations is solved by

$$\xi_j = \frac{1}{2} \left[1 + \left(\frac{1 + A}{1 - A} \right)^{N-j} \right],$$

where Eq. (31) follows for $j = 1$. Now note that $X_1 = Y_1 = \xi_1 Y_N$ but also $Y_1 = (1 + AY_N)/(1 + A)$, see above. We thereby obtain $X_1(\epsilon)$ in the quoted form [Eq. (30)], where $G_1(V)$ follows from Eqs. (4) and (10).

References

- [1] Hasan M Z and Kane C L 2010 *Rev. Mod. Phys.* **82** 3045
- [2] Qi X L and Zhang S C 2011 *Rev. Mod. Phys.* **83** 1057
- [3] Beenakker C W J 2011 preprint arXiv:1112.1950
- [4] Alicea J 2012 *Rep. Prog. Phys.* **75** 076501
- [5] Leijnse M and Flensberg K 2012 *Semicond. Sci. Techn.* **27** 124003
- [6] Lutchyn R M, Sau J D and Das Sarma S 2010 *Phys. Rev. Lett.* **105** 077001
- [7] Oreg Y, Refael G and von Oppen F 2010 *Phys. Rev. Lett.* **105** 177002
- [8] Bolech C J and Demler E 2007 *Phys. Rev. Lett.* **98** 237002
- [9] Semenoff G W and Sodano P 2007 *J. Phys. B* **40** 1479
- [10] Nilsson J, Akhmerov A R and Beenakker C W J 2008 *Phys. Rev. Lett.* **101** 120403
- [11] Law K T, Lee P A and Ng T K 2009 *Phys. Rev. Lett.* **103** 237001
- [12] Flensberg K 2010 *Phys. Rev. B* 2010 **83** 180516(R)
- [13] Wimmer M, Akhmerov A R, Dahlhaus J P and Beenakker C W J 2010 *New J. Phys.* **13** 053016
- [14] Chung S B, Qi X L, Maciejko J and Zhang S C 2011 *Phys. Rev. B* **83** 100512(R)
- [15] Golub A and Horowitz B 2011 *Phys. Rev. B* **83** 153415(R)
- [16] Bose S and Sodano P 2011 *New J. Phys.* **13** 085002
- [17] Fidkowski L, Alicea J, Lindner N H, Lutchyn R M and Fisher M P A 2012 *Phys. Rev. B* **85** 245121
- [18] Mourik V, Zuo K, Frolov S M, Plissard S R, Bakkers E P A M and Kouwenhoven L P 2012 *Science* **336** 1003
- [19] Rokhinson L, Liu X and Furdyna J 2012 *Nature Physics* **8** 795
- [20] Deng M T, Yu C L, Huang G Y, Larsson M, Caroff P and Xu H Q 2012 *Nano Lett.* **12** 6414
- [21] Das A, Ronen Y, Most Y, Oreg Y, Heiblum M and Shtrikman H 2012 *Nature Physics* **8** 887
- [22] Alicea J, Oreg Y, Refael G, von Oppen F and Fisher M P A 2011 *Nature Physics* **7** 412
- [23] Halperin B I, Oreg Y, Stern A, Refael G, Alicea J and von Oppen F 2012 *Phys. Rev. B* **85** 144501
- [24] Terhal B M, Hassler F and DiVincenzo D P 2012 *Phys. Rev. Lett.* **108** 260504
- [25] Nussinov Z, Ortiz G and Cobanera E 2012 *Phys. Rev. B* **86** 085415
- [26] Fu L 2010 *Phys. Rev. Lett.* **104** 056402
- [27] Xu C and Fu L 2010 *Phys. Rev. B* **81** 134435
- [28] Zazunov A, Levy Yeyati A and Egger R 2011 *Phys. Rev. B* **84** 165440
- [29] van Heck B, Hassler F, Akhmerov A R and Beenakker C W J 2011 *Phys. Rev. B* **84** 180502(R)
- [30] Hützen R, Zazunov A, Braunecker B, Levy Yeyati A and Egger R 2012 *Phys. Rev. Lett.* **109** 166403
- [31] van Heck B, Akhmerov A R, Hassler F, Burrello M and Beenakker C W J 2012 *New J. Phys.* **14** 035019
- [32] Béri B and Cooper N R 2012 *Phys. Rev. Lett.* **109** 156803
- [33] Hassler F and Schuricht D 2012 *New J. Phys.* **14** 125018
- [34] Béri B 2012 preprint arXiv:1212.4465
- [35] Altland A and Egger R 2012 preprint arXiv:1212.6224
- [36] Shivamoggi V, Refael G and Moore J E 2010 *Phys. Rev. B* **82** 041405(R)
- [37] Altland A and Simons B D 2010 *Condensed Matter Field Theory* (Cambridge University Press, Cambridge, UK), 2nd edition